INTERNATIONAL JOURNAL OF INTEGRATED ENGINEERING
ISSN: 2229-838X e-ISSN: 2600-7916

IJIE

Vol. 16 No. 6 (2024) 90-99
https://publisher.uthm.edu.my/ojs/index.php/ijie

# Mesh Refinement for Dynamics Airflow in Health Care

**Siti Najiah Rosminahar[1], Mohamad Nur Hidayat Mat[1]*, Eliza M. Yusup[2]**

[1] *Faculty of Mechanical Engineering, Universiti Teknologi Malaysia, 81310 UTM Johor Bahru, MALAYSIA*
[2] *Centre for NDT Training and Calibration (CENDTEC), Faculty of Mechanical and Manufacturing Engineering, Universiti Tun Hussein Onn Malaysia, 86400 Parit Raja, Johor, MALAYSIA*

*Corresponding Author: mn.hidayat@utm.my
DOI: https://doi.org/10.30880/ijie.2024.16.06.009

**Article Info**

Received: 3 April 2024
Accepted: 18 June 2024
Available online: 9 October 2024

**Keywords**

Mesh refinement, computational fluid dynamics, airborne pathogen, ventilation strategies, numerical

**Abstract**

This study explores using computational fluid dynamics (CFD) to optimize ventilation in healthcare, with a focus on mesh refinement for accurate airflow analysis. The goal is to reduce airborne contaminant spread, which is crucial during COVID-19. Ventilation in healthcare ensures air quality and minimizes pathogen transmission. The research analyzer analyzes mesh element size's impact on airflow accuracy in simulated hospital wards with two coughing patients. The optimal mesh size is determined for reliable predictions. Mesh refinement enhances accuracy in critical zones. The k-epsilon turbulence model is chosen for low error. Experimental validation shows temperature discrepancies, likely due to simulated manikins lacking clothing insulation. Air velocity measurements show minor variations within an acceptable range. Further research on various ventilation configurations and airflow rates in real hospital conditions is crucial. Addressing these limitations optimizer optimizes healthcare ventilation, enhancing safety and infection control.

## 1. Introduction

In the realm of computational fluid dynamics (CFD), the quest for accuracy in simulations is paramount, especially when applied to critical environments like healthcare facilities [1]. This paper delves into the crucial role of mesh refinement in enhancing the precision of CFD models, with a specific focus on analyzing airflow dynamics within hospital settings. During the COVID-19 pandemic, where respiratory droplet transmission has become a pressing concern, optimizing ventilation strategies to mitigate such risks is of utmost importance.

Ventilation systems serve as the lifeblood of indoor environments, facilitating air circulation and maintaining optimal air quality. Extensive research has underscored the significance of efficient ventilation strategies, particularly in high-risk settings like hospitals [2]. A study demonstrated the correlation between effective ventilation strategies and reduced transmission rates of airborne pathogens, highlighting the critical role of ventilation in infection control [3].

As the world grapples with the challenges posed by the COVID-19 pandemic, the importance of ventilation systems has garnered heightened attention [4]. Xu, Liu [5]emphasizes the necessity of robust ventilation systems in healthcare facilities, emphasizing early-stage intervention and isolation room performance. [6] further accentuate the role of ventilation in infection control within healthcare settings, stressing the need for stringent measures to minimize the risk of transmission.

However, the efficacy of ventilation systems hinges not only on air circulation but also on factors such as thermal comfort and air quality [7]. Reamer [8] cautions against overlooking ventilation standards, as negligence in adhering to guidelines can inadvertently exacerbate health risks. Petrova, Farinholt [9] advocate for

supplementary measures like high-efficiency particulate air filter (HEPA) filters to augment ventilation efficacy, particularly in healthcare facilities.

This paper seeks to address the intricacies of ventilation optimization optimization by honing in on mesh refinement techniques within CFD simulations. By leveraging advanced computational tools, we aim to elucidate the impact of mesh element size on airflow patterns and transmission risks in healthcare environments.

The specific research problem addressed in this study revolves around determining the optimal mesh element size to achieve accurate CFD simulations in healthcare settings. The aim is to bridge the gap between theoretical understanding and practical application by elucidating the relationship between mesh refinement, ventilation efficiency, and occupant comfort.

Effective ventilation strategies in hospitals should prioritize high air exchange rates to remove contaminants efficiently, prevent cross-contamination and maintain optimal temperatures for both patients and staff. The challenge lies in balancing these needs, especially considering the impact of climate change and fluctuating temperatures on thermal comfort. Therefore, achieving an optimal balance between thermal comfort and contaminant removal requires careful consideration of patient health needs. Computational Fluid Dynamics (CFD) simulations can be a valuable tool in simulating real-world scenarios with different ventilation setups to assess patient comfort levels and contaminant removal efficiency with basic setups following standard guidelines.

## 2. Methodology

The study focuses on computational modelling, boundary conditions, meshing, governing equations, mesh refinement, turbulence model selection, and experimental setup in the context of airflow dynamics within hospital environments. Computational modelling involves simulating a ward with two patients to analyze coughing particle transmission. Boundary conditions are established to emulate real-world scenarios using a simulation solver. Meshing transforms irregular areas into structured meshes, refining critical zones for detailed simulation. Governing equations, including mass, momentum, and energy conservation, are fundamental in computational fluid dynamics simulations. Mesh refinement ensures element sizes are sufficient for accuracy, employing adaptive processes to manage error tolerance. Turbulence model selection is performed to determine the most suitable model with minimal error, with the k-epsilon model chosen for its low extrapolated error. The experimental setup replicates lying positions in a well-ventilated area, measuring temperature and humidity levels to align with ventilation recommendations.

### 2.1 Computational Modelling

A ward simulating two patients is demonstrated in Fig. 1. Modular ward configurations are arranged within a hospital building, featuring two inpatient beds. This simulation replicates conditions where two patients with coughing symptoms are lying in bed. The hospital room, measuring 3m x 2.6m x 6m, is modelled in three dimensions. Inlet and outlet vents are positioned on the same side of the wall but at different heights. Both vents have identical sizes (0.4m x 0.4m). To maintain consistency with a referenced article by Ren, Wang [10] the inlet vent thickness is set at 0.05m and the outlet vent at 0.2m for this study. The dimensions of both beds are 2.0m × 0.9m × 0.12m, elevated 0.4m from the floor, with a 0.2m gap between the patients' heads and the wall behind them. The distance between the beds is fixed at 1.6m, with each bed approximately 0.6m away from the adjacent wall. In this study, the manikins representing the patients are rectangular blocks with human body and head shapes. To simulate coughing, a small circular shape representing the mouth is placed on top of each manikin's head (on the face side) with dimensions of $2cm^2$.

### 2.2 Boundary Condition

Before initiating the simulation, it is imperative to establish boundary conditions that accurately reflect the real-world scenario. The simulation solver utilised for this investigation is scFlow, a CFD tool employed to generate analytical simulations for a more comprehensive study of particle flow dynamics. As detailed in Table 1, the boundary conditions include turbulent flow set at 500 cycles to emulate a steady-state environment. Particle transmission is simulated both in steady-state and transient modes to replicate the gradual effect of human coughing. Maintaining a steady state for the initial 500 cycles enables the depiction of particle transmission and its respective sizes based on the conducted analysis. Upon transitioning to the transient mode, which simulates an individual beginning to cough, the boundary is adjusted from cycle 501 to 10,500. A Courant number of 1 is upheld, with a time step of 0.01s to enhance simulation stability. The inlet air velocity remains incompressible, while the outlet expels air at a velocity of 1m/s. The air ejected from the patient's mouth is set at 11.7m/s, with ambient temperature at 21°C and the simulated body model at 32.7°C.

Int. Journal of Integrated Engineering Vol. 16 No. 6 (2024) p. 90-99

## 2.3 Meshing

The meshing process transforms irregularly shaped or formed areas, typically found in aspect ratio studies, into element sizes during the pre-processing stage. This involves generating an unstructured mesh by iteratively dividing 3D space, with the octree parameter used to focus solely on selected experimental regions for further refinement. Notably, areas such as outlet and inlet vents for airflow profiles are refined and designated as critical. By defining specific regions for simulation, the computational load for mesh generation is reduced, resulting in higher quality meshes and decreased processing time. Ideally, fine meshing aims to produce CFD results with an error margin of less than 10%. Fig. 2 illustrates the process of refining the mesh in the inlet and outlet zones, as well as the patient's breathing zone, for detailed simulation.

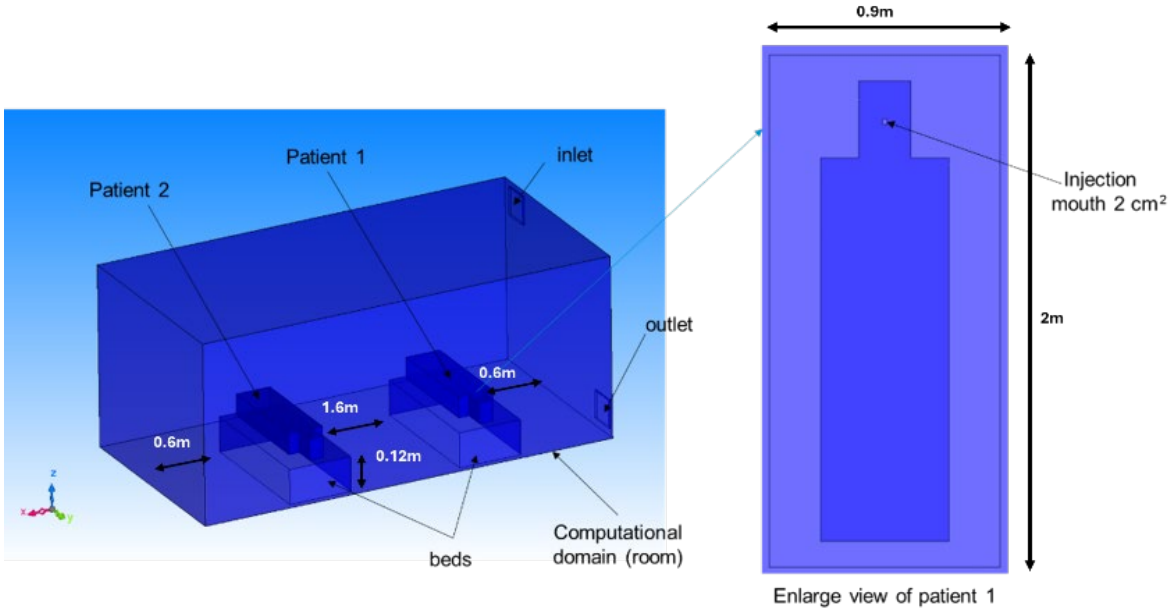


**Fig. 1** *Ward simulation set up with two patients*

**Table 1** *Boundary condition*

| Boundary | Value |
|---|---|
| Steady | 500 cycles |
| Transient | 501 - 10500 cycles |
| Time step | 0.01 s (courant number =1) |
| Turbulent model | RANS (k-epsilon) |
| Inlet exhaust | Total Pressure (Incompressible) |
| Outlet exhaust | 1 m/s (-1 direction) |
| Injector mouth | 11.7 m/s |
| Ambient temperature | 21-degree Celsius |
| Human body temperature | 36.7-degree Celsius |

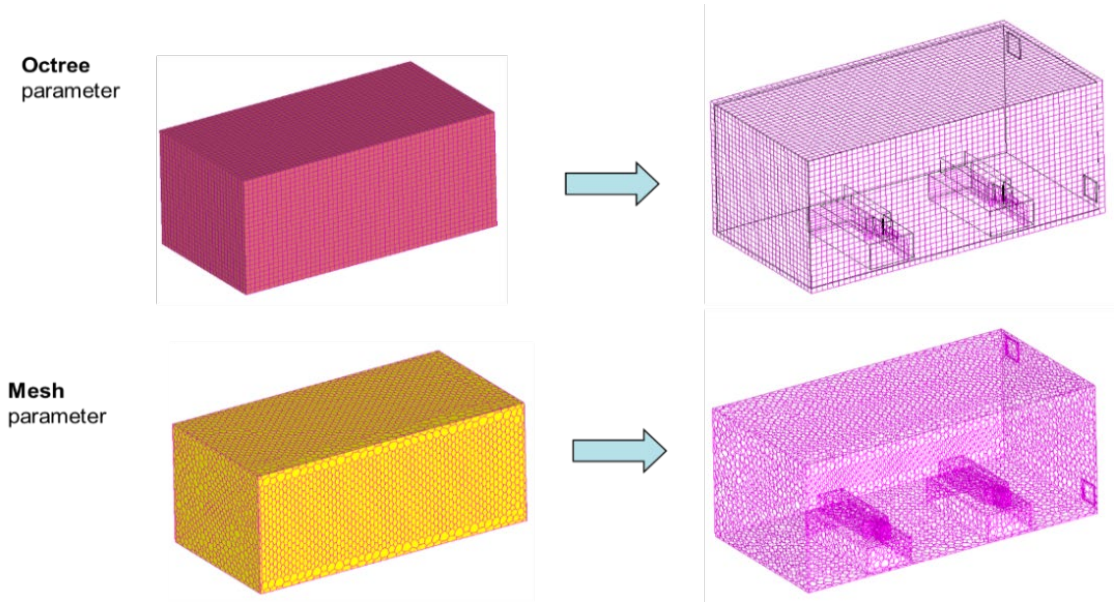


**Fig. 2** *Meshing process from octree to polyhedral mesh*

## 2.4 Governing Equation

The analysis of airflow dynamics within hospital environments relies on fundamental principles of fluid mechanics, encompassing the conservation of mass, momentum, and energy. These governing equations form the backbone of computational fluid dynamics (CFD) simulations, enabling the accurate prediction of airflow patterns and associated parameters [11].

### 2.4.1 Conservation of Mass

The continuity equation, derived from the conservation of mass principle [12], governs the flow of fluid within a given domain. In its differential form, it is expressed as:

$$\frac{\partial \rho}{\partial t} + \nabla \cdot (\rho \mathbf{u}) = 0 \tag{1}$$

Where ρ represents the density of the fluid, *u* denotes the velocity vector and ∇ signifies the divergence operator.

### 2.4.2 Conservation of Momentum

The Navier-Stokes equations encapsulate the conservation of momentum in fluid flow [13]. In their general form, they are given by:

$$\rho\left(\frac{\partial \mathbf{u}}{\partial t} + \mathbf{u} \cdot \nabla \mathbf{u}\right) = -\nabla p + \mu \nabla^2 \mathbf{u} + \mathbf{f} \tag{2}$$

Where *p* represents the pressure, *μ* denotes the dynamic viscosity of the fluid, and *f* signifies external body forces acting on the fluid.

### 2.4.3 Conservation of Energy

The conservation of energy is governed by the energy equation, which accounts for the transport of thermal energy within the fluid [14]. In its general form, it is expressed as:

$$\rho C_p \left(\frac{\partial T}{\partial t} + \mathbf{u} \cdot \nabla T\right) = \nabla \cdot (k \nabla T) + Q \tag{3}$$

Where *T* represents the temperature, $C_p$ denotes the specific heat capacity at constant pressure, *k* signifies the thermal conductivity of the fluid, and *Q* represents heat sources or sinks within the domain.

Int. Journal of Integrated Engineering Vol. 16 No. 6 (2024) p. 90-99

## 2.5 Mesh Refinement Study

This study involves conducting a mesh convergence analysis to ensure that element sizes are sufficiently obtained at key discretion points, where finer meshes are derived from the resolved model [15]. To enhance the reliability of this predictive computational model, a preliminary refinement study is initiated on the CAD model. At this stage, coarse meshes are generated as presented in Fig. 3. However, despite coarse meshes providing computational assurance for industrial applications, as noted by Bao [16], they can still present challenges in verifying accuracy due to their larger elements. Following initial iterations, the mesh refinement process begins with grids, as outlined by Zhang, Pan [17], employing higher discretization orders for the solution algorithm.

Ultimately, the accuracy of the simulation can be evaluated through refinement studies utilizing finer meshes in regions with higher stress gradients and coarser meshes in less concentrated areas of interest. Given the significance of each mesh in the computational domain relative to element sizes, adaptive refinement is proposed. In this study, an h-adaptive process is employed, subdividing each element into zones of higher and lower resolution, as suggested by Dezfooli, Khoshghalb [18], to manage permissible error tolerance. The grid spacing, denoted as h, serves as a variable representing cell length in this research. As h decreases, there is a corresponding reduction in element sizes, leading to reduced error and increased accuracy. However, variations in element sizes across generated meshes prompt consideration of the appropriate level of mesh refinement.

According to Rodrigues, de Medeiros [19], three simulations are conducted at each mesh level, with the grid refinement ratio (r) ideally being ≤ 1.1 to minimize discretization error. In most instances, proper definitions for representative cell or mesh sizes (h) are observed, with r values typically exceeding 1.3. Fig. 3 presents a graph plotting mesh convergence against velocity (m/s), providing tabulated results for different meshes: fine, medium, and coarse. In summary, the graph yields velocity values of 3.14 m/s, 3.26 m/s, 3.29 m/s, and 3.94 m/s for actual, fine, medium, and coarse meshes, respectively, concerning axial velocity (m/s). Relative error values vary depending on the study's application. In this case, a relative error value of 1.54% between the actual value and the fine mesh aims to achieve an error reading of less than 5%.

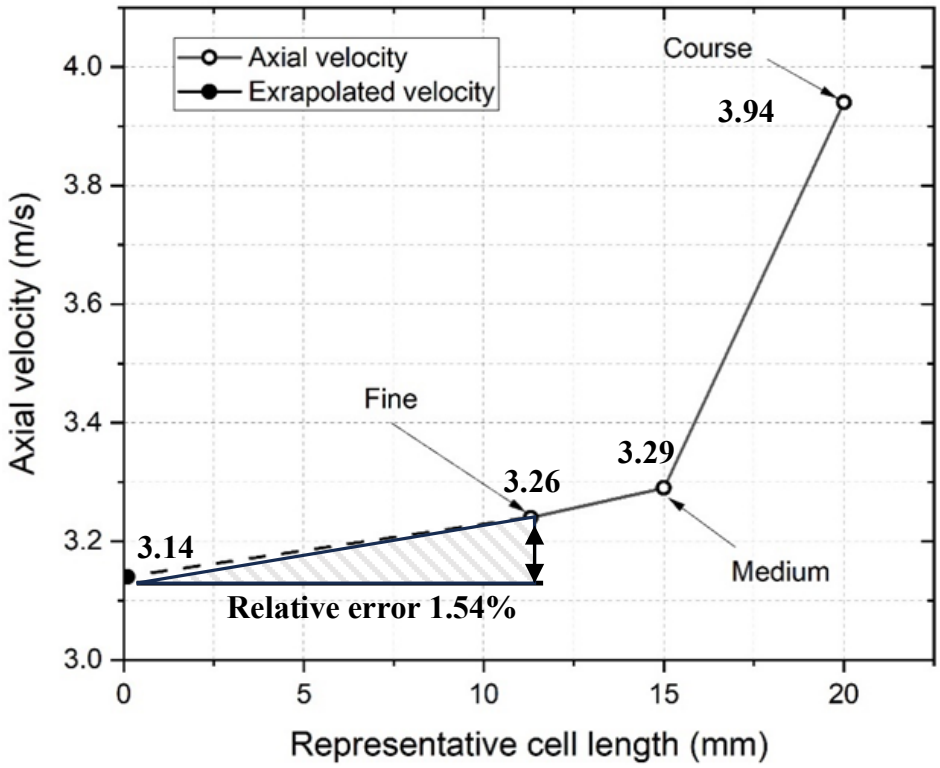


**Fig. 3** *Mesh refinement plot*

## 2.6 Turbulence Model Selection

Turbulence in fluid dynamics refers to disrupted fluid flow, causing instability among fluid particles [20]. This intricate phenomenon is analyzed through Computational Fluid Dynamics (CFD) simulations to delineate flow patterns [21]. In this investigation, various turbulent models were employed to pinpoint the most suitable one with minimal projected error. Seven turbulence models were utilized to replicate human coughing patterns. These included k-omega, MP k-epsilon, Realizable k-epsilon, RNG k-epsilon, Spalart-Allmaras, SST-V model, and standard k-epsilon. From the data presented in Table 2, it was observed that the k-epsilon model exhibited the lowest extrapolated error. Hence, it was chosen as the turbulence model for subsequent simulation studies.

***Table 2*** *Selection of turbulence model based on extrapolated errors*

| Type of turbulence model | Extrapolated errors |
|---|---|
| k-omega | 3.12 % |
| MP k-epsilon | 3.50 % |
| RealizableRealizable k-epsilon | 1.09 % |
| RNG k-epsilon | 0.71 % |
| Spalart-Allmaras | 6.98 % |
| SST-V model | 0.97 % |
| Standard k-epsilon | 0.60 % |

## 2.7 Experimental Setup

The experimental research was conducted at the UTM Health Centre (PKU) in Johor, Malaysia, situated within a meticulously ventilated environment conducive to scientific inquiry. To simulate real-world conditions, the setup emulated the lying position scenario proposed by Feng, Bi [22], as illustrated in Fig. 4. This involved positioning a 180 cm student in a supine posture on a hospital bed, oriented upward.

For precise data collection, temperature and humidity meter Habotest HT607 devices were utilized as measuring instruments in this experimental investigation. Temperature and humidity data are important as they influence airborne pathogen transmission in the indoor environment. Each sampling point underwent meticulous measurement procedures, with readings taken consecutively 10 times to ensure accuracy and reliability. Notably, the environmental conditions within the patient's vicinity were closely monitored, with temperature and humidity levels recorded at 22.91°C and 66% relative humidity, following Malaysia Department of Standard guidelines.

These measurements align with the ventilation recommendations outlined by ASHRAE [23] for occupied spaces, ensuring that the experimental setup adhered to established standards for environmental comfort and safety. By maintaining optimal conditions, the study aimed to provide robust and representative data for analysis, contributing to a comprehensive understanding of ventilation dynamics in healthcare settings.

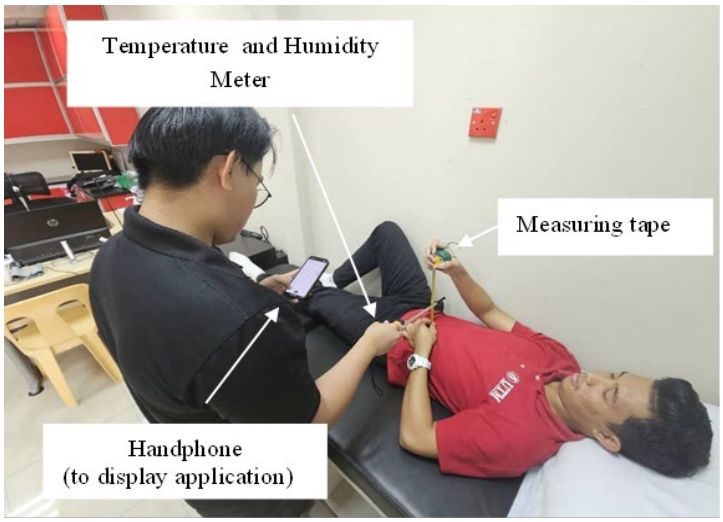


**Fig. 4** *Experimental setup for temperature and humidity data sampling*

Fig. 5 provides a visual representation of the meticulous placement of measuring points within the simulated environment. These measuring points are strategically positioned at 10-cm intervals, meticulously spanning from ground level (0cm) to a height of 50cm above the floor. To ensure comprehensive data collection and analysis, particularly about human presence and interaction with the airflow patterns, the measuring points are intelligently subdivided into six distinct sections. This subdivision is achieved by considering the relative height of an average human being, which is approximately 180cm. Leveraging this human-centric perspective, the measuring points are segmented using Relative Human Height (RHH) values. These RHH values, ranging from 0.2 to 1.00, effectively divide the height range into sections that correspond to different levels of human presence within the environment.

Specifically, these sections are demarcated at intervals that correspond to 20%, 40%, 60%, 80%, 94%, and 100% of the average human height, respectively. By adopting this approach, the measuring points capture data at

Int. Journal of Integrated Engineering Vol. 16 No. 6 (2024) p. 90-99

various heights relative to the typical standing posture of an individual, enabling a nuanced understanding of airflow dynamics and distribution within the simulated space.

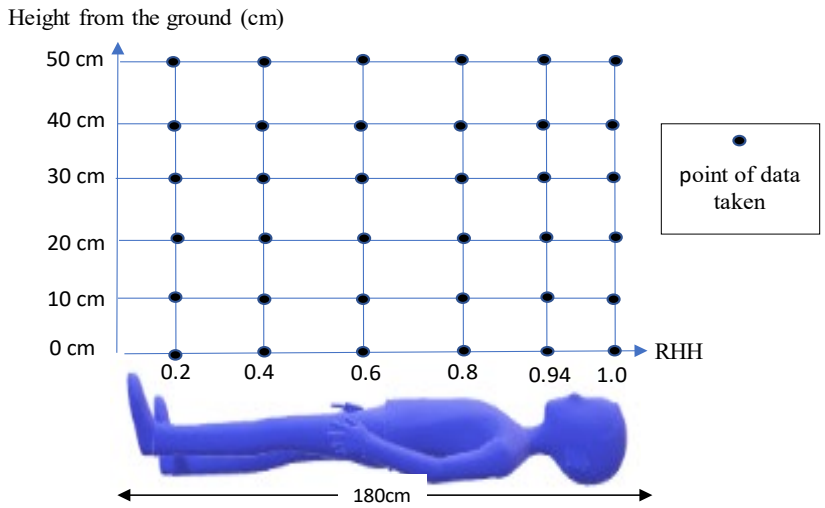


**Fig. 5** *Location point of data sampling*

## 3. Result and Discussion

### 3.1 Temperature Over Relative Human Height

In the simulation study, the standard K-epsilon turbulence model is utilized to capture turbulent flow phenomena accurately. The positioning of manikins is established horizontally within the computational domain to simulate realistic scenarios. Sampling points are strategically placed at intervals of 0cm, 10cm, 20cm, 30cm, 40cm, and 50cm relative to human height (RHH) values ranging from 0.2 to 1.00. These sampling points are crucial for assessing the airflow dynamics and thermal behavior at various heights within the simulated environment.
To maintain consistency with the experimental setup, input parameters such as temperature and velocity are kept constant. The distances between sampling points for each case are meticulously determined based on the RHH, aligning with the experimental sampling point locations to ensure accurate comparison between experimental and simulated data.

Fig. 5 illustrates the comparison between experimental and simulated values at specific points presented in Fig. 6. The comparison is repeated for 10°C,20°C,30°C and 40 °C subsequently. It is observed that the experimental temperatures consistently fall within the range of 23 to 24°C on average, adhering to the indoor room temperature standards established by the Departments of Standards Malaysia [120]. However, the simulated temperature values exhibit notable deviations, ranging from 27 to 35°C. This disparity can be attributed to the absence of clothing insulation on the simulated manikins, which is a crucial factor affecting thermal comfort. According to ASHRAE [121], bedding materials contribute significantly to thermal insulation when an individual is at rest, effectively regulating body temperature. However, this aspect is not considered in the simulation setup. Incorporating appropriate bedding materials in the simulation could potentially enhance the accuracy of simulated temperatures, bringing them closer to the experimental readings and ensuring a more realistic representation of thermal conditions within the simulated environment.

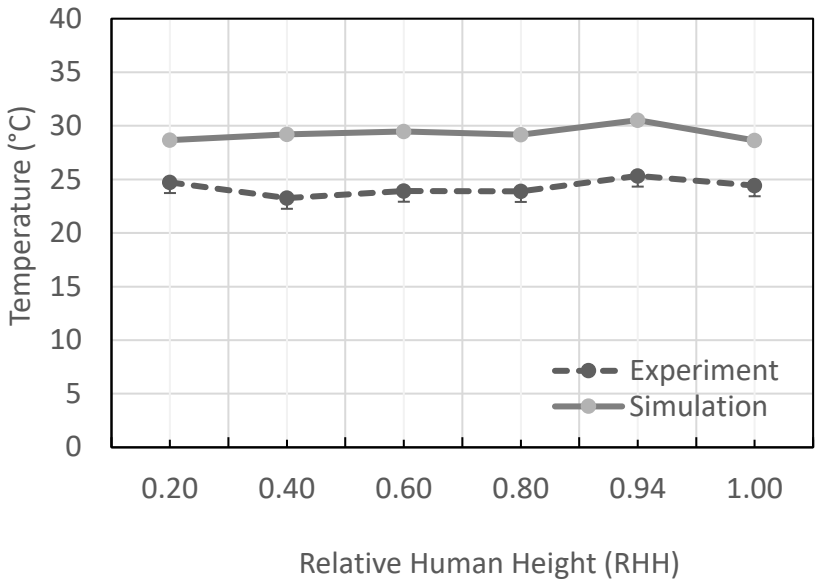


**Fig. 6** *Validation for temperature relative to human height at 0 cm from the ground*

## 3.2 Air Velocity Over Relative Human Height

Comparative data readings between experimental and simulation setups are determined to observe any significant dissimilarities. Any notable differences will highlight the accuracy of the simulation result grounded on the same airflow velocity. Fig. 7 illustrates the sampling points chosen to measure velocity parameters at various locations compared to the reference point depicted in Fig. 6. This experimental procedure is replicated at intervals of 10cm, ranging from 10cm to 50cm above the ground. The velocity graph shows a steady, almost similar linear trend for most of the sampling points at the primary level. An ideal trend demands both simulation and experimental sampling values to be imposed on each other or share the same pattern at the very least. As the distance of the measuring tools progresses further, the gap between experimental and simulation sampling values is higher. An instrument glitch might influence this profound finding. The device can capture value in certain ranges with a specific predetermined reading value. At the rate of precision, simulation sampling values are more diverse in values of range, creating more options for the numerical value being displayed. Although both setups show discrepancies, the difference is minimal and lies under an acceptable margin.

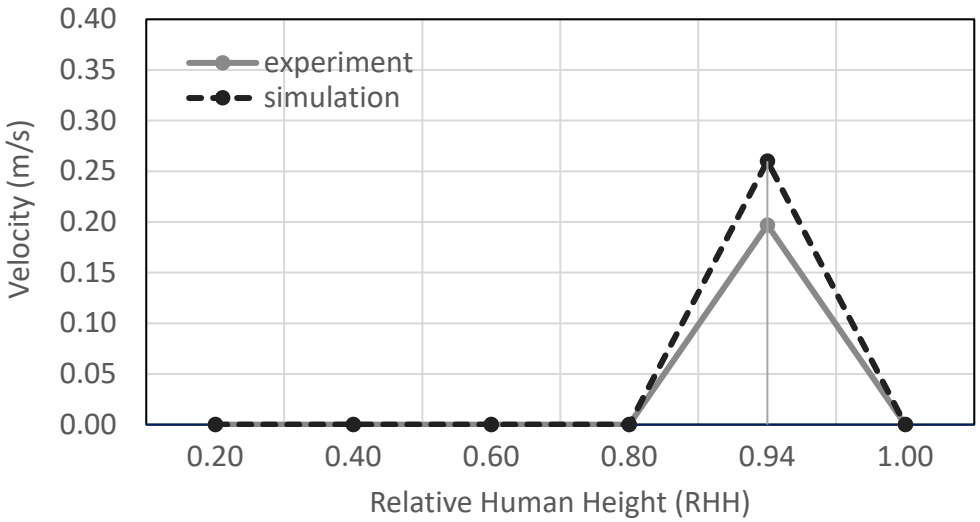


**Fig. 7** *Validation for velocity relative to human height at 0 cm from the ground*

## 3.3 Air Flow Velocity For 2 Cases

The airflow simulation in terms of velocity streamlines from inlet to outlet for two (2) cases set with air changes per hour ACH 61.3 can be seen in Fig. 8. In other words, around 61 times the air is renewed in the room within a one-hour duration. The airflow pattern for case 1, as in Fig. 8a shows a circulation pattern starting from the inlet

Int. Journal of Integrated Engineering Vol. 16 No. 6 (2024) p. 90-99

surface to the outlet. This is due to the location of the inlet and the outlet situated on the same wall side. Thus, it induces flow rotation within the room. The air velocity streamlines' magnitude can be differentiated by its streamlined length. At the inlet, the velocity magnitude is higher and reduces its magnitude when approaching obstacles, which are the walls, beds and mannikins. Based on this flow pattern, the air is mixed within the room before exiting the outlet. Meanwhile, for case 2 in Fig. 8a, which is under stratum ventilation settings, the airflow initially goes from the inlet to the outlet, and there is less mixed circulation within the room. The airflow that does not directly exit the outlet reverses, and little recirculates before leaving the outlet.

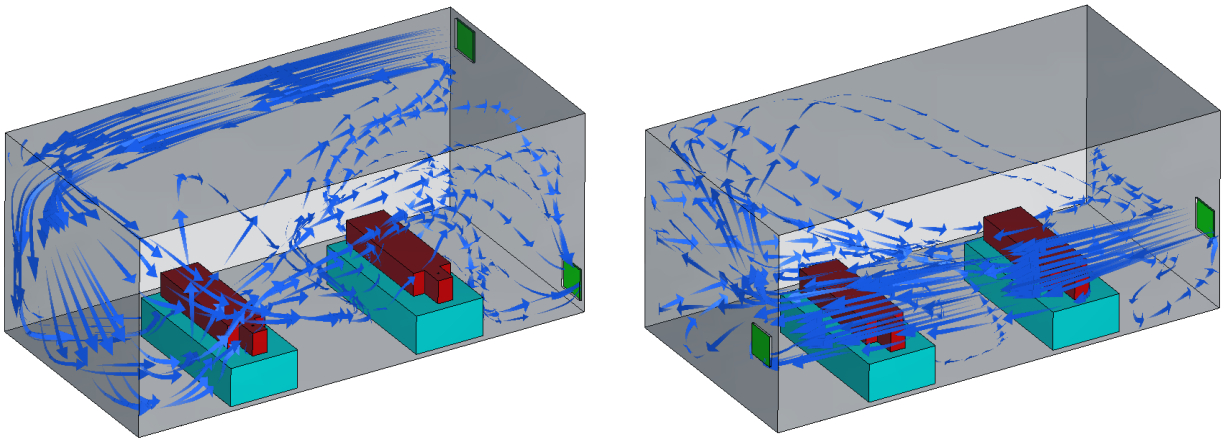

**(a)** **(b)**

**Fig. 8** *Air flow pattern for 2 cases: (a) Circulation airflow; (b) Stratum airflow*

## Conclusion

This study investigated the efficacy of utilizing computational fluid dynamics (CFD) simulations for optimizing ventilation strategies in healthcare facilities, specifically focusing on balancing thermal comfort and contaminant removal. The research employed a systematic approach, integrating experimental measurements with CFD simulations to analyze airflow dynamics within a simulated hospital ward. The k-epsilon turbulence model demonstrated the lowest extrapolated error and was chosen for subsequent simulations. Differences were observed between simulated and experimental temperature readings, likely attributable to no clothing insulation worn by simulated manikins. Incorporating bedding materials in future simulations could improve the accuracy of thermal comfort predictions. While both experimental and simulated air velocity measurements exhibited slight variations, the differences remained within an acceptable margin.

Future studies could incorporate realistic clothing insulation factors to enhance the accuracy of thermal comfort predictions. Further research is warranted to explore the impact of various ventilation configurations and airflow rates on both contaminant removal and thermal comfort within healthcare settings. Additionally, investigations into the efficacy of ventilation strategies in mitigating the airborne transmission of viruses in dynamic airflow scenarios prevalent in real-world hospital environments are crucial. By addressing these limitations and pursuing the suggested research avenues, future studies can contribute significantly to optimizing ventilation strategies in healthcare facilities. This optimization will ultimately promote patient safety, staff well-being, and improved infection control within these critical environments.

## Acknowledgement

This research was sponsored by the Ministry of Higher Education (MOHE) of Malaysia through the Fundamental Research Grant Scheme (FRGS/1/2021/TK0/UTM/02/98).

## Conflict of Interest

The authors declare that there is no conflict of interest regarding the publication of the paper.

## Author Contribution

*The authors confirm contributions to the paper as follows****: study conception and design****: Siti Najiah, Mohamad Nur Hidayat;* ***data collection****: Siti Najiah;* ***analysis and interpretation of results****: Siti Najiah, Mohamad Nur Hidayat, Eliza M. Yusup;* ***draft manuscript preparation****: Siti Najiah, Eliza M. Yusup. All authors reviewed the results and approved the final version of the manuscript.*

## References


[1] Tu, J., et al., *Computational fluid dynamics: a practical approach*. 2023: Elsevier.
[2] O'Keeffe, J., et al., *COVID-19 and indoor air: risk mitigating measures and future-proofing*. 2021: BC Centre for Disease Control.
[3] Sadrizadeh, S., et al., *A systematic review of operating room ventilation.* Journal of Building Engineering, 2021. 40: p. 102693.
[4] Gaffar, S.A. and N. Khan, *Enhancing Indoor Air Quality: Optimizing Air-Conditioning And Ventilation Systems Amidst The Global Coronavirus Epidemic.* Journal of Survey in Fisheries Sciences, 2022: p. 802-812.
[5] Xu, C., et al., *Prediction and control of aerosol transmission of SARS-CoV-2 in ventilated context: from source to receptor.* Sustainable cities and society, 2022. 76: p. 103416.
[6] Tushar, S.R., et al., *Driving sustainable healthcare service management in the hospital sector.* Journal of Cleaner Production, 2023. 420: p. 138310.
[7] Cheong, K., et al., *Thermal comfort study of an air-conditioned lecture theatre in the tropics.* Building and environment, 2003. 38(1): p. 63-73.
[8] Reamer, F.G., *Risk management in the behavioral health professions: A practical guide to preventing malpractice and licensing-board complaints*. 2023: Columbia University Press.
[9] Petrova, E., et al., *A community-based management of COVID-19 in a mobile container unit.* Vaccines, 2021. 9(11): p. 1362.
[10] Ren, J., et al., *Numerical study of three ventilation strategies in a prefabricated COVID-19 inpatient ward.* Building and Environment, 2021. 188: p. 107467.
[11] Zawawi, M.H., et al. *A review: Fundamentals of computational fluid dynamics (CFD)*. in *AIP conference proceedings*. 2018. AIP Publishing.
[12] Hafeez, H.Y. and C.E. Ndikilar, *4.1 The continuity equation.* Applications of Heat, Mass and Fluid Boundary Layers, 2020: p. 67.
[13] Ranjan, R. and C. Pantano, *A collocated method for the incompressible Navier–Stokes equations inspired by the Box scheme.* Journal of Computational Physics, 2013. 232(1): p. 346-382.
[14] Yuhua, F., *New Newton Mechanics Taking Law of Conservation of Energy as Unique Source Law.* Science Journal of Physics, 2015. 2013.
[15] Pisarciuc, C., I. Dan, and R. Cioară, *The Influence of Mesh Density on the Results Obtained by Finite Element Analysis of Complex Bodies.* Materials, 2023. 16(7): p. 2555.
[16] Bao, H., *Development of a Data-driven Framework for Mesh-Model Optimization in System-level Thermal-Hydraulic Simulation*. 2018: North Carolina State University.
[17] Zhang, W., et al., *An efficient tree-topological local mesh refinement on Cartesian grids for multiple moving objects in incompressible flow.* Journal of Computational Physics, 2023. 479: p. 111983.
[18] Dezfooli, M.S., et al., *An h-adaptive edge-based smoothed point interpolation method for elasto-plastic analysis of saturated porous media.* Computers and Geotechnics, 2023. 162: p. 105628.
[19] Rodrigues, A.L.B., J.B. de Medeiros, and E.S. Benta, *GRID CONVERGENCE TEST FOR A BI-DIMENSIONAL HYPERSONIC FLOW SIMULATION.* JP Journal of Heat and Mass Transfer, 2023. 35: p. 125-137.
[20] Avila, M., D. Barkley, and B. Hof, *Transition to turbulence in pipe flow.* Annual Review of Fluid Mechanics, 2023. 55: p. 575-602.
[21] Liang, Q., et al., *Simulating Microscale Urban Airflow and Pollutant Distributions Based on Computational Fluid Dynamics Model: A Review.* Toxics, 2023. 11(11): p. 927.
[22] Feng, G., et al., *Study on the motion law of aerosols produced by human respiration under the action of thermal plume of different intensities.* Sustainable cities and society, 2020. 54: p. 101935.
[23] Zuhaib, S., et al., *An Indoor Environmental Quality (IEQ) assessment of a partially-retrofitted university building.* Building and Environment, 2018. 139: p. 69-85.